Inorganic Chemistry

Article

pubs.acs.org/IC

Mild Hydrothermal Crystal Growth, Structure, and Magnetic Properties of Ternary U(IV) Containing Fluorides: $LiUF_5$, KU_2F_9, $K_7U_6F_{31}$, $RbUF_5$, RbU_2F_9, and RbU_3F_{13}

Jeongho Yeon,[†] Mark D. Smith,[†] Joshua Tapp,[‡] Angela Möller,[‡] and Hans-Conrad zur Loye*[,†]

[†]Department of Chemistry and Biochemistry, University of South Carolina, Columbia, South Carolina 29208, United States

[‡]Department of Chemistry, University of Houston, Houston, Texas 77204, United States

Supporting Information

ABSTRACT: Single crystals of several ternary alkali uranium fluorides, $LiUF_5$, KU_2F_9, $K_7U_6F_{31}$, $RbUF_5$, RbU_2F_9, and RbU_3F_{13}, have been obtained in a mild hydrothermal process using $UO_2(CH_3CO_2)_2(H_2O)_2$ as the uranium source. Their crystal structures were determined by single crystal X-ray diffraction. The uranium in the starting reagent was successfully reduced from U^{6+} to U^{4+} in a dilute hydrofluoric acid environment, aided by the presence of a copper salt. All materials exhibit highly complex crystal structures that range from two-dimensional to three-dimensional. The U^{4+} cations are found in high (UF_8 and UF_9) coordination environments. The magnetic susceptibility measurements yielded effective magnetic moments of 3.01−3.83 μ_B for the U^{4+} cations. The temperature dependent magnetic susceptibility measurements confirmed that the U^{4+} cation exhibits a nonmagnetic singlet ground state at low temperatures. No long-range magnetic order was observed for any of the above compositions down to 2 K. Optical and thermal behaviors of the fluorides were also investigated.

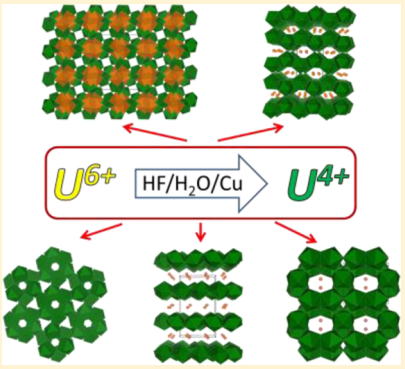

INTRODUCTION

U(IV) containing fluorides are of particular interest among the many uranium containing materials due to their important roles in uranium separation and in the production of uranium oxides that are currently being used in the uranium enrichment process to create nuclear fuel.[1−6] Furthermore, investigations of U(IV) in fluoride hosts is of interest because of potential optical properties exhibited by these materials, such as luminescence, that may find use in applications ranging from UV solid-state lasers to visible light emitting phosphors.[7−11]

Among the known U(IV) fluoride materials, the ternary alkali U(IV) fluorides are the most studied, and approximately 30 ternary inorganic U(IV) fluorides have been reported to date.[12−31] Some information on the structurally characterized U(IV) fluorides is found in Table S1. Polycrystalline powders or single crystals of the reported U(IV) fluorides were usually prepared by precipitation from aqueous solutions or by crystallization in high temperature flux reactions using alkali fluoride/chloride salts. Although two crystal structures of the title compounds were previously reported,[26,29] little information beyond their chemical compositions, if that, was reported for the other members. Reports on these fluorides are over 30 years old, and many include only very rudimentary crystallographic data (see Table 1). Furthermore, almost no measurements of their physical properties were carried out, motivating the desire to prepare single crystals of these and other reduced U(IV) fluorides in order to carry out high quality structure and physical property determinations.[32−34]

The extremely rich crystal chemistry of U(IV) fluorides is due to the presence of large coordination environments of the U(IV) cation, and the different connectivity modes between the UF_x polyhedra. For these reasons, several distinct structure types are found among the U(IV) fluorides, including isolated units,[25,28,30,31] chains,[23,27,31] sheets,[17,19,20,22] and frameworks,[13−15,24,26,29] composed of UF_x polyhedra, resulting in simple zero-dimensional to complex three-dimensional crystal structures. Due to the presence of unpaired f electrons, it is desirable to explore their electronic and/or magnetic properties.[32−34]

We are particularly interested in further expanding the use of our new synthetic route to incorporate U(IV) species in extended fluoride structures. Recently, we found that U(IV) containing fluorides can be readily synthesized via an in situ reduction step taking place under mild hydrothermal conditions at relatively low temperatures.[35] Using this synthetic method, we previously reported several binary and quaternary U(IV) fluorides.[35,36] Specifically for the synthesis of $U_3F_{12}(H_2O)$, the U(VI) in the starting reagent ($UO_2(CH_3CO_2)_2(H_2O)_2$) was successfully reduced to U(IV) in a dilute hydrofluoric acid environment, where the presence of a copper salt was essential to crystallize the $U_3F_{12}(H_2O)$ phase. To study the utility of this method for the synthesis of other new U(IV) fluorides, we undertook a systematic study of ternary U(IV) fluorides to explore this phase space. Utilizing $UO_2(CH_3CO_2)_2(H_2O)_2$ as a

Received: April 10, 2014
Published: May 27, 2014

   dx.doi.org/10.1021/ic5008507 | Inorg. Chem. 2014, 53, 6289−6298

Table 1. A List of the Known Structural Information for the Reported U(IV) Fluorides in This Work[a]

			lattice parameters					
	space group	product type	a/Å	b/Å	c/Å	β/°	R factor	year
$LiUF_5$	$I4_1/a$	single crystal	14.884	14.884	6.547		0.072	1966[29]
	$I4_1/a$	single crystal	14.8467(7)	14.8467(7)	6.5168(6)		0.028	this work
KU_2F_9	$Pnma$	single crystal	8.7021(9)	11.4769(4)	7.0350(3)		0.068	1969[26]
	$Pnma$	single crystal	8.6923(6)	11.4542(8)	7.0132(5)		0.025	this work
$K_7U_6F_{31}$	N/A	powder						1996[16]
	$R\bar{3}$	single crystal	15.1426(8)	15.1426(8)	10.386(1)		0.039	this work
$RbUF_5$	N/A	powder						1996[16]
	$P2_1/c$	single crystal	8.2407(5)	13.7275(5)	8.3295(3)	102.447(1)	0.036	this work
RbU_2F_9	$Pnma$	single crystal	8.7330(8)	11.675(1)	7.0304(6)		0.030	this work
RbU_3F_{13}	$Pmc2_1$	single crystal	7.9943(6)	7.3217(5)	8.4677(6)		0.040	this work

$LiUF_5$[29]		KU_2F_9[26]	
U(1)−F(2)	2.26(2)	U(1)−F(5)	2.292(1)
U(1)−F(5)	2.26(2)	U(1)−F(1)	2.30(2)
U(1)−F(4)	2.27(2)	U(1)−F(2)	2.32(2)
U(1)−F(3)	2.30(1)	U(1)−F(1)	2.32(2)
U(1)−F(4)	2.31(2)	U(1)−F(3)	2.32(2)
U(1)−F(1)	2.31(2)	U(1)−F(4)	2.33(2)
U(1)−F(3)	2.34(1)	U(1)−F(4)	2.34(2)
U(1)−F(1)	2.47(2)	U(1)−F(2)	2.34(2)
U(1)−F(2)	2.59(2)	U(1)−F(3)	2.39(2)

[a]The U−F bond distances for the known $LiUF_5$ and KU_2F_9 are also listed to compare them with the data from this work, which shows that overall quality of the data is significantly improved over the known data.

starting reagent, based on the synthetic approach we developed, we were able to grow high quality single crystals of several U(IV) fluorides in excellent yield. Although some of the title compounds are known, the structure determinations reported herein are significantly improved over the limited amount of information that had been published. Also, the successful application of this entirely different synthetic route to prepare these fluorides suggests that this approach can readily be extended to the preparation of numerous other U(IV) containing fluorides. In this paper, we report on the synthesis, crystal structures, and magnetic properties of several ternary alkali U(IV) containing fluorides.

EXPERIMENTAL SECTION

Reagents. $UO_2(CH_3CO_2)_2{\cdot}2H_2O$ (International Bio-Analytical Industries, Inc. ACS grade), LiF (Alfa Aesar, 98+%), KF (Alfa Aesar, 99%), RbF (Alfa Aesar, 99.7%), $Cu(CH_3CO_2)_2{\cdot}2H_2O$ (Aldrich, 98+%), and HF (Alfa Aesar, 48%) were used as received.

Synthesis. Single crystals of the reported materials were grown via a mild hydrothermal route. For all compositions, 1 mmol of $UO_2(CH_3CO_2)_2{\cdot}2H_2O$, 0.5 mmol of $Cu(CH_3CO_2)_2{\cdot}2H_2O$, 1 mL of H_2O, and 1 mL of HF were used. To these mixtures, 2 mmol of LiF, 0.7 mmol of KF, 4 mmol of KF, 0.5 mmol of RbF, and 4 mmol of RbF were added to prepare $LiUF_5$, KU_2F_9, $K_7U_6F_{31}$, RbU_3F_{13}, and $RbUF_5$, respectively. RbU_2F_9 was obtained as a secondary product during the synthesis of both RbU_3F_{13} and $RbUF_5$. Specific reaction conditions are summarized in Table 2.

The respective solutions were placed into 23 mL Teflon-lined autoclaves. The autoclaves were closed, heated to 200 °C at a rate of 5 °C min^{-1}, held for 1 day, and cooled to room temperature at a rate of 6 °C h^{-1}. The mother liquor was decanted from the single crystal products, which were isolated by filtration and washed with distilled water and acetone. The reactions, except for RbU_3F_{13} and $RbUF_5$, yielded a single phase product consisting of green crystals in a nearly quantitative yield based on $UO_2(CH_3CO_2)_2{\cdot}2H_2O$. In all cases, Cu metal powder was also generated and selectively removed by dissolving it in concentrated HNO_3. As illustrated in Figure S1, the powder X-ray diffraction patterns of the ground crystals indicate that no impurities are contained in the products.

Table 2. Specific Reaction Conditions for the Syntheses of the Reported Materials[a]

	molar ratios			
A^+	A	U	Cu	product(s)
Li	1	1	0.5	$LiUF_5$
	4	1	0.5	$LiUF_5$
K	0.5	1	0.5	$KU_2F_9 + U_3F_{12}(H_2O)$[35]
	0.7	1	0.5	KU_2F_9
	2	1	0.5	$KU_2F_9 + K_7U_6F_{31}$
	4	1	0.5	$K_7U_6F_{31}$
Rb	0.5	1	0.5	RbU_3F_{13}
	2	1	0.5	$RbU_2F_9 + RbU_3F_{13}$
	2.5	1	0.5	$RbU_2F_9 + RbU_3F_{13} + RbUF_5$
	3	1	0.5	$RbU_3F_{13} + RbUF_5$
	4	1	0.5	$RbUF_5$

[a]All reactions were performed at 200 °C.

Single Crystal X-ray Diffraction. X-ray intensity data from green crystals were collected at either 100(2) or 295(2) K using a Bruker SMART APEX diffractometer (Mo Kα radiation, λ = 0.71073 Å).[37] The data collection covered a minimum of 99.7% of reciprocal space to $2\theta_{max}$ = 66.3−72.8°, with R_{int} = 0.043−0.056 after absorption correction. The raw area detector data frames were reduced and corrected for absorption effects with the SAINT+ and SADABS programs.[37] Final unit cell parameters were determined by least-squares refinement of large sets of reflections taken from the data set. Direct-methods structure solution, difference-Fourier calculations, and full-matrix least-squares refinement against F^2 were performed with SHELXS/L as implemented in OLEX2.[38,39]

For all materials, the respective space groups were determined by the pattern of systematic absences in the intensity data and by structure solution. It should be noted that one F atom in $K_7U_6F_{31}$ is disordered about Wyckoff site 3a with 3 site symmetry, generating six 1/6-occupied atomic positions per cavity site. Free refinement of both

dx.doi.org/10.1021/ic5008507 | Inorg. Chem. 2014, 53, 6289−6298

Table 3. Crystallographic Data for $LiUF_5$, KU_2F_9, $K_7U_6F_{31}$, RbU_2F_9, $RbUF_5$, and RbU_3F_{13}

formula	$LiUF_5$	KU_2F_9	$K_7U_6F_{31}$	$RbUF_5$	RbU_2F_9	RbU_3F_{13}
fw	339.97	686.16	2290.88	418.50	732.53	1046.56
temp (K)	100(2)	100(2)	295(2)	295(2)	100(2)	100(2)
cryst syst	tetragonal	orthorhombic	trigonal	monoclinic	orthorhombic	orthorhombic
space group	$I4_1/a$	*Pnma*	$R\bar{3}$	$P2_1/c$	*Pnma*	$Pmc2_1$
a (Å)	14.8467(7)	8.6923(6)	15.1426(8)	8.2407(3)	8.7330(8)	7.9943(6)
b (Å)	14.8467(7)	11.4542(8)	15.1426(8)	13.7275(5)	11.675(1)	7.3217(5)
c (Å)	6.5168(6)	7.0132(5)	10.386(1)	8.3295(3)	7.0304(6)	8.4677(6)
β (deg)				102.447(1)		
V (Å^3)	1436.5(2)	698.26(8)	2062.4(3)	920.12(6)	716.8(1)	495.63(6)
Z	16	4	3	8	4	2
density (g/cm^3)	6.418	6.527	5.534	6.042	6.788	7.013
abs coeff (mm^{-1})	45.177	47.039	36.475	45.783	51.986	53.939
cryst size (mm^3)	0.10 × 0.06 × 0.05	0.10 × 0.04 × 0.02	0.06 × 0.04 × 0.03	0.48 × 0.04 × 0.02	0.10 × 0.08 × 0.07	0.10 × 0.06 × 0.05
2 θ range (deg)	5.48−70.0	6.82−72.7	5.00−66.3	5.06−68.1	6.76−72.6	4.82−72.8
reflns collected	16 778	20 268	16 928	24 717	21 276	14 717
data/restraints/params	1587/0/65	1760/0/58	1756/0/70	3751/0/127	1804/0/59	2490/1/90
R (int)	0.0447	0.0434	0.0556	0.0508	0.0511	0.0493
GOF (F^2)	1.301	1.155	1.109	1.031	1.146	1.056
R (F)[a]	0.0279	0.0251	0.0395	0.0358	0.0301	0.0400
R_w (F_0^2)[b]	0.0570	0.0623	0.1008	0.0742	0.0725	0.1038

[a] $R(F) = \Sigma||F_o| - |F_c||/\Sigma|F_o|$. [b] $R_w(F_0^2) = [\Sigma w(F_o^2 - F_c^2)^2/\Sigma w(F_o^2)^2]^{1/2}$.

Table 4. Selected Interatomic Distances (Å) for $LiUF_5$, KU_2F_9, $K_7U_6F_{31}$, RbU_2F_9, $RbUF_5$, and RbU_3F_{13}

$LiUF_5$		KU_2F_9		$K_7U_6F_{31}$		RbU_2F_9	
U(1)−F(2)	2.224(4)	U(1)−F(5)	2.2879(2)	U(1)−F(2)	2.183(5)	U(1)−F(1)	2.284(3)
U(1)−F(4)	2.261(3)	U(1)−F(1)	2.300(2)	U(1)−F(4)	2.187(5)	U(1)−F(2)	2.294(3)
U(1)−F(5)	2.271(3)	U(1)−F(4)	2.307(3)	U(1)−F(3)	2.294(5)	U(1)−F(4)	2.317(3)
U(1)−F(4)	2.296(3)	U(1)−F(2)	2.311(3)	U(1)−F(3)	2.301(5)	U(1)−F(5)	2.3180(3)
U(1)−F(3)	2.299(3)	U(1)−F(3)	2.322(3)	U(1)−F(5)	2.308(5)	U(1)−F(1)	2.336(3)
U(1)−F(1)	2.320(3)	U(1)−F(1)	2.327(3)	U(1)−F(5)	2.345(5)	U(1)−F(3)	2.343(3)
U(1)−F(3)	2.349(3)	U(1)−F(2)	2.339(3)	U(1)−F(1)	2.369(4)	U(1)−F(2)	2.346(3)
U(1)−F(1)	2.453(4)	U(1)−F(4)	2.359(3)	U(1)−F(1)	2.374(4)	U(1)−F(3)	2.370(3)
U(1)−F(2)	2.578(4)	U(1)−F(3)	2.385(3)			U(1)−F(4)	2.383(3)
$RbUF_5$				RbU_3F_{13}			
U(1)−F(4)	2.145(4)	U(2)−F(1)	2.470(4)	U(1)−F(1)	2.298(6)	U(2)−F(1)	2.285(6)
U(1)−F(2)	2.157(4)	U(2)−F(1)	2.787(4)	U(1)−F(2)	2.375(5)	U(2)−F(1)	2.285(6)
U(1)−F(5)	2.299(4)	U(2)−F(3)	2.312(4)	U(1)−F(3)	2.268(6)	U(2)−F(2)	2.271(6)
U(1)−F(3)	2.304(4)	U(2)−F(6)	2.381(4)	U(1)−F(4)	2.347(6)	U(2)−F(2)	2.271(6)
U(1)−F(5)	2.333(4)	U(2)−F(7)	2.385(4)	U(1)−F(4)	2.280(6)	U(2)−F(3)	2.457(6)
U(1)−F(6)	2.363(4)	U(2)−F(8)	2.157(4)	U(1)−F(5)	2.319(5)	U(2)−F(3)	2.457(6)
U(1)−F(1)	2.410(4)	U(2)−F(9)	2.161(4)	U(1)−F(6)	2.350(4)	U(2)−F(8)	2.400(8)
U(1)−F(7)	2.498(4)	U(2)−F(10)	2.298(4)	U(1)−F(7)	2.291(5)	U(2)−F(9)	2.307(9)
U(1)−F(7)	2.670(4)	U(2)−F(10)	2.278(4)	U(1)−F(8)	2.427(4)	U(2)−F(9)	2.247(9)

the site occupancy and displacement parameters gave physically senseless results because of high correlation between these two parameters. Fixing the occupancy at 1/6 is physically sensible (not more than 100% occupancy relative to the ordered site) and gives a charge-neutral composition. The larger displacement parameter of F(6) reflects its higher positional uncertainty as a consequence of site disorder. All atoms except the disordered F(6) atom were refined with anisotropic parameters. Crystallographic data, selected interatomic distances, and atomic coordinates are listed in Tables 3 and 4 and in the Supporting Information, respectively.

Powder X-ray Diffraction. Powder X-ray diffraction data were collected on a Rigaku D/Max-2100 powder X-ray diffractometer using Cu Kα radiation. The step-scan covered the angular range 10−70° 2θ in steps of 0.04°. No impurities were observed, and the calculated and experimental PXRD patterns are in good agreement.

UV−Vis Diffuse Reflectance Spectroscopy. Diffuse reflectance spectra of polycrystalline powder samples of the reported materials were obtained using a PerkinElmer Lambda 35 UV/vis scanning spectrophotometer equipped with an integrating sphere in the range 200−900 nm. The reflectance data were converted to absorbance data using Kubelka−Munk function.[40]

Magnetic Property Measurements. The magnetic properties of the microcrystalline compounds were measured using a Quantum Design Physical Property measurement System (QD-PPMS) equipped with a vibrating-sample magnetometer. Temperature dependent susceptibility measurements were made in both zero-field cooled (ZFC) and field cooled (FC) conditions in applied fields of 1000 Oe. Magnetization measurements at 2 K were carried out in applied fields up to 8 T.

RESULTS AND DISCUSSION

Synthesis. Single crystals of ternary U(IV) fluorides were historically obtained via crystal growth in high temperature (*T*

dx.doi.org/10.1021/ic5008507 | Inorg. Chem. 2014, 53, 6289−6298

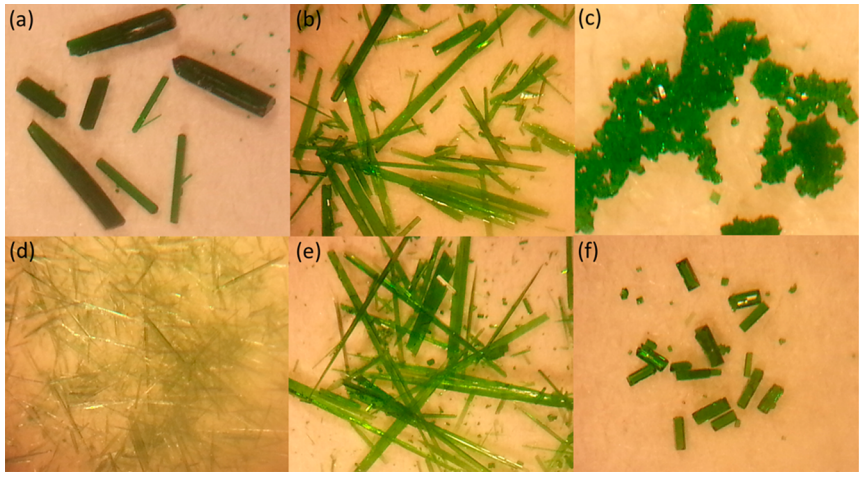

Figure 1. Optical images of single crystal for (a) $LiUF_5$, (b) KU_2F_9, (c) $K_7U_6F_{31}$, (d) $RbUF_5$, (e) RbU_2F_9, and (f) RbU_3F_{13}. The maximum crystal size is approximately 2 mm.

> 500 °C) molten alkali fluoride/chloride salts using UF_4 as a starting reagent.[19,24,26,27,29,30] In some cases, such as the ammonium containing U(IV) fluorides, they were obtained as byproducts during the hydrothermal synthesis of organic–inorganic hybrid materials involving several organic reducing reagents.[14,15] Our group has modified the latter method and developed a mild hydrothermal route using $UO_2(CH_3CO_2)_2(H_2O)_2$ as a starting reagent, because the acetate species (the reducing agent) is already incorporated into the uranium source, eliminating the need for additional reducing agents. Using this method, we have explored the phase space of alkali U(IV) fluorides by systematically changing the A/U ratios (A = alkali metals) since the resultant product composition is very sensitive to the molar ratios of the reagents, as summarized in Table 2. It is important to note that the presence of a copper salt is necessary to crystallize the title materials, as reported in our previous work, since the copper is believed to be involved in the catalytic reduction of U(VI) to U(IV).[35]

The investigation of the Li–U–F system yielded $LiUF_5$ as the sole product from all the reactions we explored. In the K–U–F and Rb–U–F systems, however, several phases were obtained in each case from the different reactions that were explored. It is interesting to note that some products were formed over a wide range of A/U ratios. For example, KU_2F_9 and RbU_3F_{13} appeared in the A/U ratios of 0.5/1 to 2/1 and 0.5/1 to 3/1, respectively. Also, it should be noted that the final compositions were not those of the initial A/U ratios; in other words, uranium rich phases, such as KU_2F_9, RbU_2F_9, and RbU_3F_{13}, could be obtained from uranium poor reaction ratios.

For all cases, the U(VI) in the starting reagent was successfully reduced to the U(IV), and high quality single crystals were obtained, as demonstrated in Figure 1. In all reactions, copper metal was formed as a byproduct that was selectively removed by dissolving it in concentrated nitric acid. Single phase products could be obtained for almost all compositions by optimizing the A/U ratio of the starting reagents, the exception being RbU_2F_9. Powder X-ray diffraction patterns of the ground crystals confirmed the purity of the reported ternary U(IV) fluorides as illustrated in Figure S1. No ternary U(IV) fluorides containing sodium were isolated due to the stability of the quaternary $Na_4CuU_6F_{30}$ phase,[36] which formed preferentially. Despite several attempts, we were unable to obtain any cesium containing fluorides.

Structure. $LiUF_5$ crystallizes in the tetragonal space group $I4_1/a$, consistent with the previously reported data (see Table 1).[29] $LiUF_5$ exhibits a complex crystal structure consisting of corner-, edge-, or face-shared UF_9 and LiF_6 polyhedra (see Figure 2). The crystal structure can be divided into two parts,

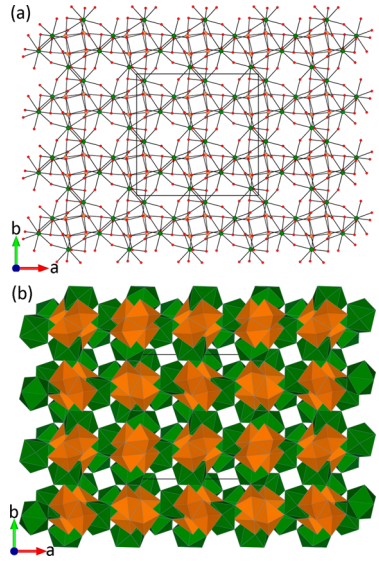

Figure 2. Ball-and-stick and polyhedral representations of $LiUF_5$ along the *c* axis. The three-dimensional structure consists of corner-, edge-, and face-shared UF_9 and LiF_6 polyhedra. The green, orange, and red spheres/polyhedra represent U^{4+}, Li^+, and F^- ions, respectively.

the arrangement of (1) the UF_9 and of (2) the LiF_6 polyhedra. The first part is a complex three-dimensional network composed of only UF_9 polyhedra as shown in Figure 3, where a tetrameric building block of $U_4F_{30}^{14-}$ is found. The tetramer is formed from four corner-shared UF_9 polyhedra, two of which also engage in edge-sharing in the middle of the tetramer. Each tetramer is oriented perpendicular to the *ab* plane and is connected to other tetramers via edge-sharing. The tetramers stack along the *c* axis via edge-sharing, which creates two types of square channels, as illustrated in Figure 3b. The larger channels are filled by $Li_4F_{16}^{12-}$ tetramers, whereas the

dx.doi.org/10.1021/ic5008507 | Inorg. Chem. 2014, 53, 6289–6298

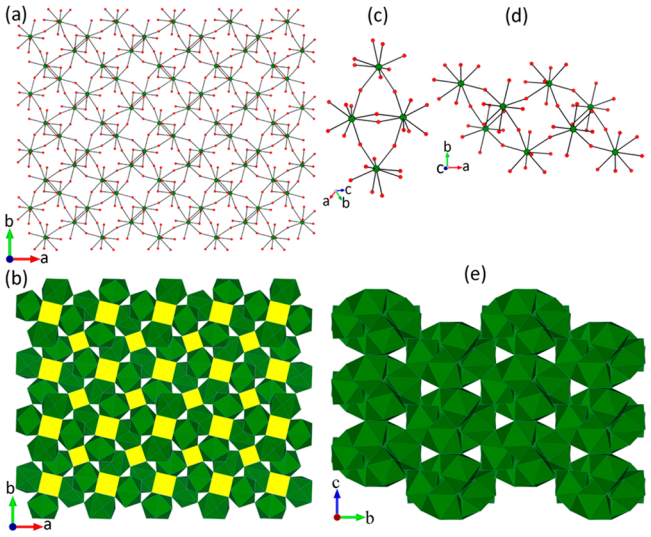

Figure 3. $LiUF_5$. The arrangement of the UF_9 polyhedra (a and b), where the U_4F_{30} tetramers (c and d) create square channels along the *c* axis represented by the yellow squares. The UF_9 polyhedra also arrange into larger clusters (e). Green and red spheres represent the U^{4+} and F^- ions, respectively.

smaller channels persist along the *c* direction (Figure 2b). The arrangement of the UF_9 polyhedra results in ellipsoidal clusters that are stacked along the *c* axis as shown in Figure 3e. The cluster consists of two corner-shared $U_4F_{30}^{14-}$ tetramers (see Figure 3d), forming a square space that is eventually occupied by the $Li_4F_{16}^{12-}$ tetramers. The second part of the structure consists of an arrangement of isolated $Li_4F_{16}^{12-}$ tetramers. Each tetramer is made up of four edge-shared LiF_6 polyhedra, creating a distorted cube that fills the aforementioned square void.

In the structure, the U^{4+} cation is surrounded by nine fluorine atoms to form a distorted tricapped trigonal prismatic coordination environment with U−F distances ranging from 2.224(4) Å to 2.578(4) Å. Each UF_9 polyhedron shares its corners with four other U^{4+} and four Li^+ cations, edges with two U^{4+} and one Li^+ cation(s), and a face with one Li^+ cation (see Figure 4c). The Li^+ cation is found in an irregular LiF_6 octahedron, with Li−F distances ranging from 1.876(13) Å to 2.218(13) Å. Each LiF_6 polyhedron shares its corners with four U^{4+} cations, an edge with one U^{4+}, three edges with other Li^+ cation(s), and a face with one U^{4+} cation (see Figure 4d). Bond valence sum calculations[41,42] resulted in values of 1.00 and 3.89 for Li^+ and U^{4+} cations, respectively, consistent with the expected values.

AU_2F_9 (A = K^+ and Rb^+) crystallizes in the orthorhombic space group of *Pnma*. The structure of KU_2F_9 is consistent with previously reported data (see Table 1),[26] but RbU_2F_9 is a new member of the U(IV) fluoride family. The two compositions exhibit a complex three-dimensional crystal structure consisting of corner- and edge-shared UF_9 polyhedra, as shown in Figure 5. The three-dimensional framework is built up from puckered two-dimensional sheets in the *ac* plane that are stacked along the *b* axis through corner-sharing. This connectivity results in elongated hexagonally shaped channels in which the A^+ cations reside. The sheets are composed of zigzag chains, which run along the *a* axis and that are connected via corner- and edge-sharing to each other, resulting in the puckered layers in the *ac* plane shown in Figure 6a and b.

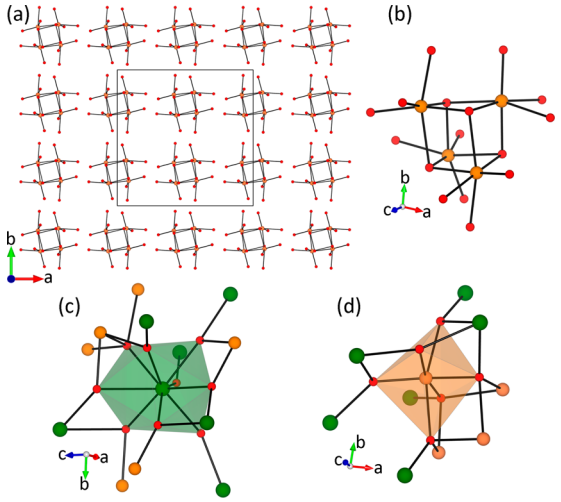

Figure 4. Illustration of the arrangement of the $[LiF_{3/1}F_{3/3}]_4$ tetramers consisting of edge-shared LiF_6 polyhedra (a), which creates a distorted cube (b). The local coordination environments of the UF_9 and LiF_6, and the connectivity to other metal cations around the polyhedra, are shown in c and d, respectively. Green, orange, and red spheres indicate the U^{4+}, Li^+, and F^- ions, respectively.

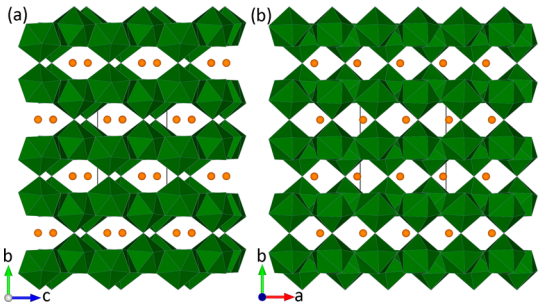

Figure 5. Illustration of polyhedral representations of AU_2F_9 (A = K, Rb) along the (a) *a* and (b) *c* axes, which shows a three-dimensional crystal structure consisting of corner- and edge-shared UF_9 polyhedra. The framework is formed by the corner-sharing of two-dimensional sheets along the *b* axis. The green and orange polyhedra/spheres are U^{4+} and A^+ cations, respectively.

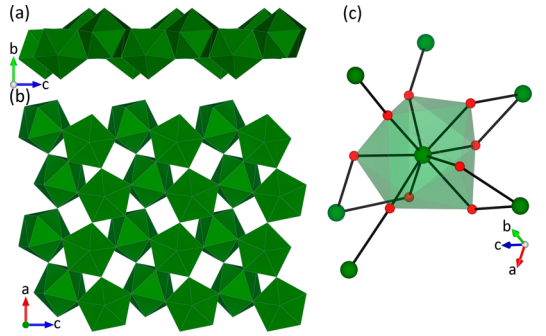

Figure 6. Two different views of the two-dimensional layers found in AU_2F_9 (A = K, Rb), where the layer is created by edge-sharing one-dimensional chains that consists of corner-sharing UF_9 polyhedra running along the *a* axis (a and b). The local coordination environment is shown in c, representing a distorted tricapped trigonal prism of the U^{4+} cation.

The U^{4+} cation is coordinated to nine fluorine atoms forming a distorted tricapped trigonal prism with U−F distances ranging from 2.284(3) Å to 2.385(3) Å (see Figure 6c). The A^+ cations

dx.doi.org/10.1021/ic5008507 | *Inorg. Chem.* 2014, 53, 6289−6298

are found in irregular AF_9 polyhedra with A−F distances ranging from 2.614(3) Å to 3.187(3) Å and 2.691(3) Å to 3.177(4) Å for KF_9 and RbF_9, respectively. Bond valence sum calculations[41,42] resulted in values of 1.09−1.12 and 3.68−3.75 for the A^+ and the U^{4+} cations, respectively, consistent with the expected values.

Although the composition $K_7U_6F_{31}$ has appeared in the literature, no additional information was reported.[16] $K_7U_6F_{31}$ crystallizes in the trigonal space group of $R\bar{3}$, isostructural with $(NH_4)_7U_6F_{31}$[15] and $Na_7Zr_6F_{31}$,[43] and exhibits a complex three-dimensional crystal structure consisting of corner- and edge-shared UF_8 polyhedra, as shown in Figure 7. The most

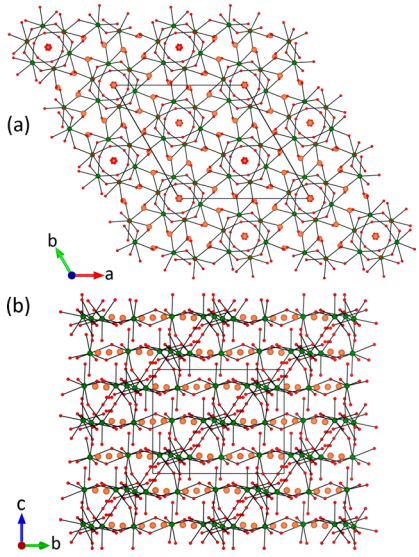

Figure 7. Ball-and-stick representations of the structure of $K_7U_6F_{31}$, where the basic building block, the hexameric $[UF_{4/1}F_{4/2}]_6$ group, can be seen in a and b. In a, disordered F^- atoms are observed inside the hexamers along the *c* axis. Green, orange, and red polyhedra/spheres represent U^{4+}, Rb^+, and F^- ions, respectively.

interesting structural feature of this material is the presence of a cuboctahedral cluster, which is made up of six corner-shared UF_8 polyhedra, as shown in Figure 8a and b. Each cluster is surrounded by six additional clusters, all of which share their edges and build up a three-dimensional framework that contains hexagonal channels along the *c* axis, as illustrated in Figure 8d and e. The K^+ cations reside within the channels and between the clusters.

The structure of $K_7U_6F_{31}$ can also be described as a three-dimensional network composed of layers, as shown in Figure 9. In each layer, the edge-shared U_2F_{16} dimers are connected to each other via corner-sharing to form planar sheets; this connectivity results in 12-membered rings within the slabs. Subsequent layers are linked through corner-sharing and staggered along the *c* axis such that the 12-membered rings are not aligned; instead the staggered arrangement of the layers creates hexagonal channels that are formed by the clusters, as mentioned earlier.

In the hexagonal channels as shown in Figures 7a and 8e, the F(6) atom is disordered over six sites and makes long contacts with surrounding U^{4+} cations. Interestingly, in $Na_7Zr_6F_{31}$,[43] isostructural with $K_7U_6F_{31}$, the fluorine atom in the same hexagonal channels is located in the center of the channel without any locational disorder. This difference is likely due to

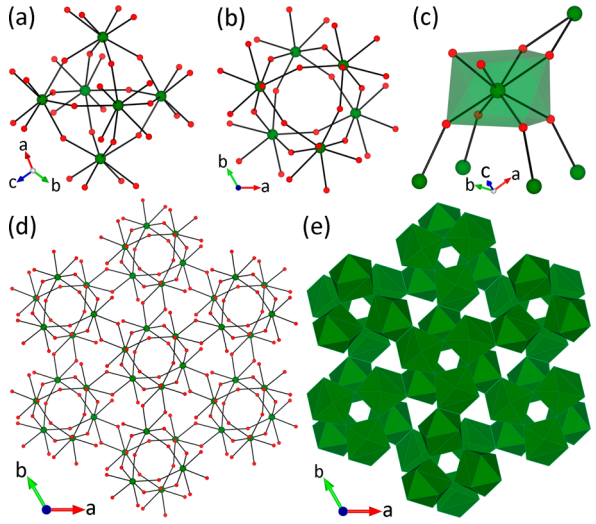

Figure 8. Hexameric building blocks found in $K_7U_6F_{31}$ (a and b) and their connectivity, illustrated in d and e, which creates hexagonal channels along the *c* axis, in which K^+ and disordered F^- ions reside. The U^{4+} cation is observed in a distorted square antiprismatic coordination environment as shown in c.

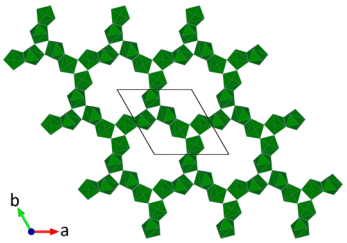

Figure 9. Arrangement of the UF_8 polyhedra in the *ab* plane forming a two-dimensional sheet containing 12-membered rings.

the larger size of the U^{4+} cation that prefers a larger coordination environment compared to Zr^{4+}.

The U^{4+} cation is found in a distorted square antiprismatic coordination environment (see Figure 8c) with U−F distances ranging from 2.183(5) Å to 2.374(4) Å. This coordination sphere, quite different from those found for the other fluorides reported here, may affect the magnetic properties of $K_7U_6F_{31}$, which is discussed below. The $K(1)^+$ cations are located between the clusters, whereas $K(2)^+$ cations reside in the hexagonal channels. Both K^+ cations are observed in irregular polyhedra with K−F distances ranging from 2.647(5) Å to 3.356(6) Å. Bond valence sum calculations[41,42] resulted in values of 1.00−1.11 and 4.07 for the K^+ and U^{4+} cations, respectively, consistent with the expected values.

$RbUF_5$ crystallizes in a monoclinic space group of $P2_1/c$ and is isostructural with $TlUF_5$.[17] Although the existence of $RbUF_5$ was reported earlier from powder diffraction data, its crystal structure has never been analyzed. $RbUF_5$ exhibits a layered structure consisting of corner-, edge-, and face-shared UF_9 polyhedra as illustrated in Figure 10. The layers are separated by the Rb^+ cations along the *b* axis. As shown in Figure 11a and b, the two-dimensional features are composed of double chains containing UF_9 polyhedra that are connected to each other via corner-sharing to form layers in the *ac* plane. Each ribbon is created from the edge-sharing between the one-dimensional connectivity of the UF_9 polyhedra that propagate along the *c* axis. These linear chains are then linked together via edge- and

dx.doi.org/10.1021/ic5008507 | Inorg. Chem. 2014, 53, 6289−6298

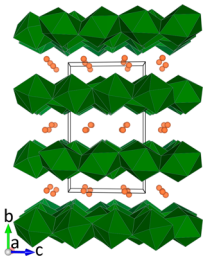

Figure 10. Illustration of the polyhedral structure of $RbUF_5$, where layers are separated by the Rb^+ cations. Green and orange polyhedra/spheres represent U^{4+} and Rb^+ cations, respectively.

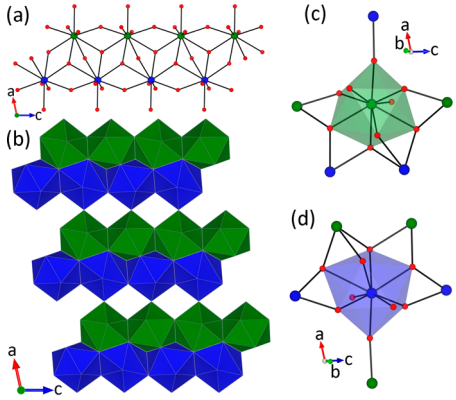

Figure 11. Illustration of a sheet of $RbUF_5$ in the *ac* plane. The layers in b are composed of corner-shared double chains in a that are formed by the edge- and face-sharing of one-dimensional single chains consisting of edge-shared UF_9 polyhedra. Both $U(1)^{4+}$ and $U(2)^{4+}$ cations exhibit a distorted tricapped trigonal prismatic coordination environment as shown in c and d. Green and blue polyhedra/spheres indicate U(1) and U(2), respectively.

face-sharing between the UF_9 polyhedra. It is worth pointing out that $RbUF_5$ includes connectivities of corner-, edge-, and face-sharing between the UF_9 polyhedra, which is a rare bonding mode in ternary U(IV) fluorides.

There are two crystallographically unique U^{4+} cations in $RbUF_5$, both of which are found in a similar distorted tricapped trigonal prismatic coordination environment (Figure 11c and d) with U−F distances ranging from 2.145(4) Å to 2.787(4) Å. Both $Rb(1)^+$ and $Rb(2)^+$ cations are surrounded by nine fluorine atoms forming irregular polyhedra with Rb−F distances between 2.785(4) Å and 3.376(4) Å. Bond valence sum calculations[41,42] resulted in values of 0.81 and 3.97−4.03 for the Rb^+ and U^{4+} cations, respectively, which are consistent with the expected values.

RbU_3F_{13} crystallizes in the noncentrosymmetric orthorhombic space group of $Pmc2_1$, is isostructural with $RbTh_3F_{13}$,[44] and exhibits a three-dimensional connectivity composed of corner- and edge-shared UF_9 polyhedra as shown Figure 12. The Rb^+ cations reside in the hexagonal-like channels created by the $U_3F_{13}^-$ framework that contains two crystallographically unique U^{4+} cations. The three-dimensional framework can be considered a combination of two structural parts, layers and chains consisting of the $U(1)F_9$ and $U(2)F_9$ polyhedra, respectively. The $U(1)F_9$ polyhedra are connected to each other via corner-sharing along the *c* axis and via edge-sharing along the *a* axis, which results in the slightly puckered layers stacked along the *b* axis as illustrated in Figure 13a and b. The chains consist of corner-shared $U(2)F_9$ polyhedra running

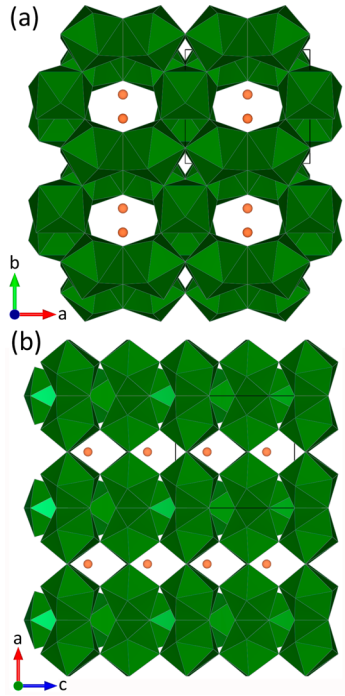

Figure 12. Polyhedral representation of the crystal structure of RbU_3F_{13} consisting of corner- and edge-shared UF_9 polyhedra. Green and orange polyhedra/spheres represent the U^{4+} and Rb^+ cations, respectively.

along the *c* axis (see Figure 13c), and these chains link the layers along the *b* axis via corner- and edge-sharing, forming the three-dimensional crystal structure shown in Figures 13d and e.

Both $U(1)^{4+}$ and $U(2)^{4+}$ cations are observed in similar distorted tricapped trigonal prismatic UF_9 polyhedra with U−F bond distances ranging from 2.247(9) Å to 2.457(6) Å. The local coordination environments and connectivity to adjacent atoms for each U^{4+} cation are shown in Figure 13f and g. Nine fluorine atoms surround the rubidium cation with Rb−F distances between 2.755(9) Å and 3.168(7) Å. Bond valence sum calculations[41,42] resulted in values of 0.84 and 3.84−4.14 for Rb^+ and U^{4+} cations, respectively, which are consistent with the expected values.

UV−Vis Diffuse Reflectance Spectroscopy. UV−vis diffuse reflectance data were measured on ground crystals of the reported materials and were converted to absorbance using the Kubelka−Munk function.[40] As shown in Figure 14, all spectra are similar to each other, where the absorption bands are attributed to the f−f transitions in the U^{4+} cation. The bands above 400 nm are due to f−f transitions, including transitions from the ground state, of $^3H_4$ to several excited states such as $^1I_6$, $^3P_1$, $^1G_4$, $^1D_2$, $^3P_0$, $^3H_6$, $^3H_4$, etc. The observed spectra are consistent with those obtained for previously reported materials[35,45−48] and confirmed the presence of the U(IV). The band gaps estimated by the onset of the absorption edge resulted in values of 3.9−4.2 eV, suggesting an insulating nature of the reported materials.

Thermal Behavior. The thermal behaviors of the reported materials were investigated by heating the samples in air to examine the formation of potential single-phase oxide materials when the fluorides are thermally treated. All samples were heated to 800 °C in air, and the products after heating were characterized by powder X-ray diffraction (PXRD). PXRD analyses determined that the thermal products consisted of

dx.doi.org/10.1021/ic5008507 | Inorg. Chem. 2014, 53, 6289−6298

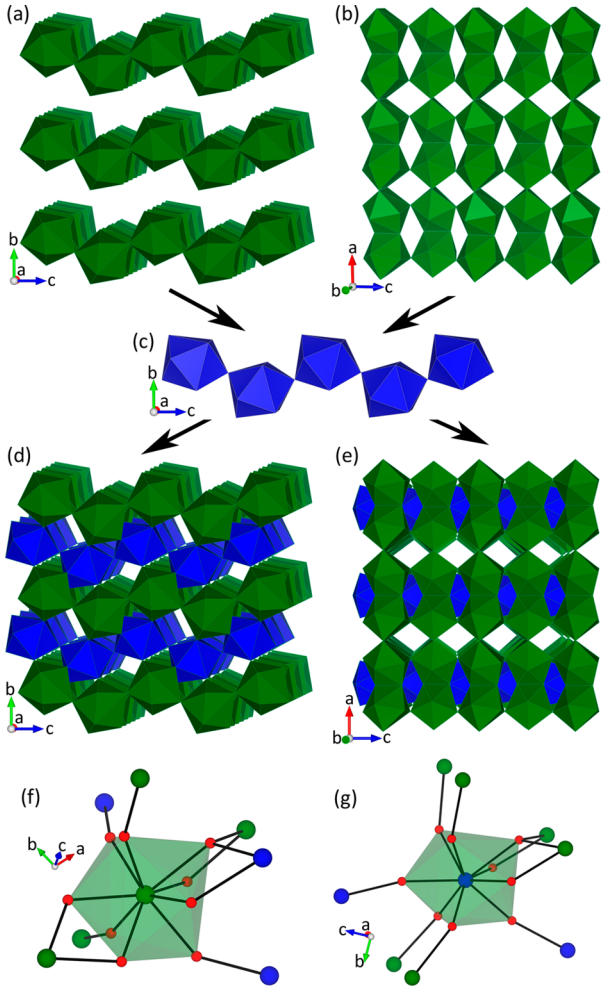

Figure 13. Layers consisting of edge-shared U(1)F_9 polyhedra in a and b in the *ac* plane, which are connected to chains of corner-shared U(2)F_9 polyhedra in c via corner- and edge-sharing, thereby creating the framework in d and e. The local coordination environments of the U(1) and U(2) cations are shown in f and g, respectively. Green and blue polyhedra represent U(1)F_9 and U(2)F_9, respectively.

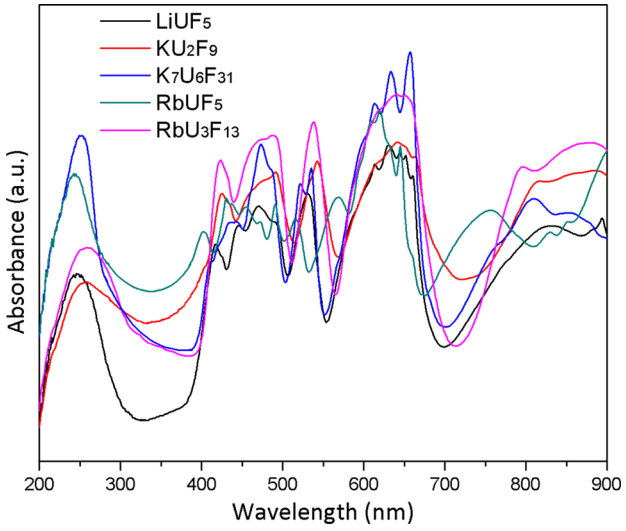

Figure 14. UV–vis absorbance spectra for the reported materials.

$Li_{22}U_{18}O_{65}$,[49] $LiU_{0.83}O_3$,[50] $K_2U_2O_7$,[51] $Rb_2U_2O_7$,[52] $Rb_2U_4O_{13}$,[53] and $Rb_4U_5O_{17}$[54] as the major phases and at least one additional unidentified minor phase. Perhaps not unexpected, it turns out that the reported alkali U(IV) fluorides are thermally converted to a mixture of several U(VI) oxides due to oxidation of U(IV) to U(VI) at high temperatures in air.

Magnetic Properties. The magnetic susceptibilities of the title U(IV) fluorides were investigated over the temperature range of 2–350 K, in an applied field of 1000 Oe. For all materials, no differences are observed between zero field cooled (zfc) and field cooled (fc) data, and the data similarly reflect magnetic contributions from only U^{4+} cations. No long-range ordering was evidenced down to 2 K.

As shown in Figure 15, the magnetic susceptibilities increase with decreasing temperature and begin to deviate strongly from

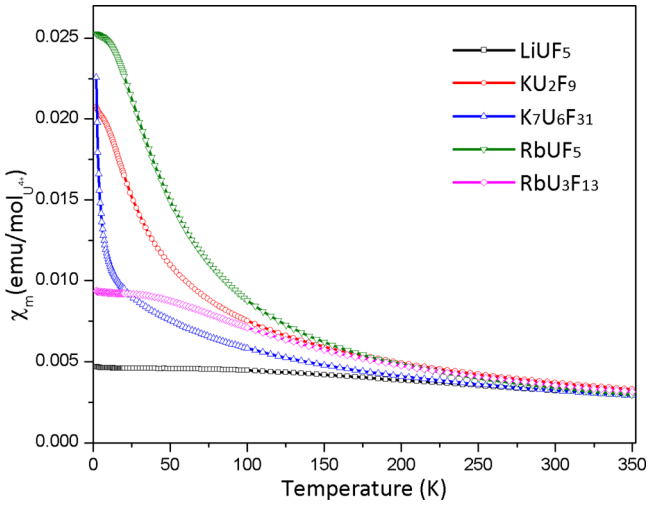

Figure 15. Temperature dependence of the magnetic susceptibility data for $LiUF_5$, KU_2F_9, $K_7U_6F_{31}$, $RbUF_5$, and RbU_3F_{13} measured in an applied field of 1000 Oe.

the Curie–Weiss law starting at approximately 100–200 K, most likely due to the depopulation of thermally accessible excited states and the formation of a singlet ground state of the U^{4+} cation at low temperatures. $K_7U_6F_{31}$ is an exception to this behavior and exhibits temperature dependent behavior down to low temperatures, see also field dependent magnetization measurements shown in the Supporting Information. Temperature independent paramagnetic behavior at low temperature is a typical characteristic of the U^{4+} cation and originates from the coupling between a nonmagnetic ground state and low lying excited states through Zeeman perturbation.[55,56]

As seen in Figure S2, the inverse susceptibility data in the linear high temperature region were fitted to the Curie–Weiss law, $\chi = C/(T - \theta)$, where C is the Curie constant and θ is the paramagnetic Weiss constant. The constants extracted from the fits are listed in Table 5. Effective magnetic moments of 3.01–3.83 μ_B for the U^{4+} cation are obtained, which are slightly smaller and larger than the expected value of 3.58 μ_B calculated from Russell–Saunders coupling for a $^3H_4$ ground state, but are still consistent with previously reported data.[57−60] Figure S3 shows the magnetization of the compounds measured in various applied fields, where a linear trend is found, indicating the absence of field dependent behavior, e.g. saturation of magnetic moments. Among the reported fluorides, $K_7U_6F_{31}$ exhibits a quite unexpected result, reproducible paramagnetic behavior at low temperatures, and this abnormal feature is clearly apparent in Figure 16. A derivative of the inverse

dx.doi.org/10.1021/ic5008507 | Inorg. Chem. 2014, 53, 6289–6298

Table 5. Constants Extracted from the Magnetic Susceptibility Data for $LiUF_5$, KU_2F_9, $K_7U_6F_{31}$, $RbUF_5$, and RbU_3F_{13}[a]

	C (emu·K·mol^{-1})	θ (K)	μ_{eff}/μ_B per U^{4+}
$LiUF_5$	1.84(3)	−272(1)	3.83(3)
KU_2F_9	2.98(1)	−102.9(2)	3.45(1)
$K_7U_6F_{31}$	8.88(1)	−159(3)	3.44(1)
$RbUF_5$	1.13(1)	−30.1(5)	3.01(1)
RbU_3F_{13}	4.22(1)	−95.9(1)	3.35(1)

[a] C, θ, and μ_{eff} represent the Curie constant, the Weiss constant, and the effective magnetic moment, respectively.

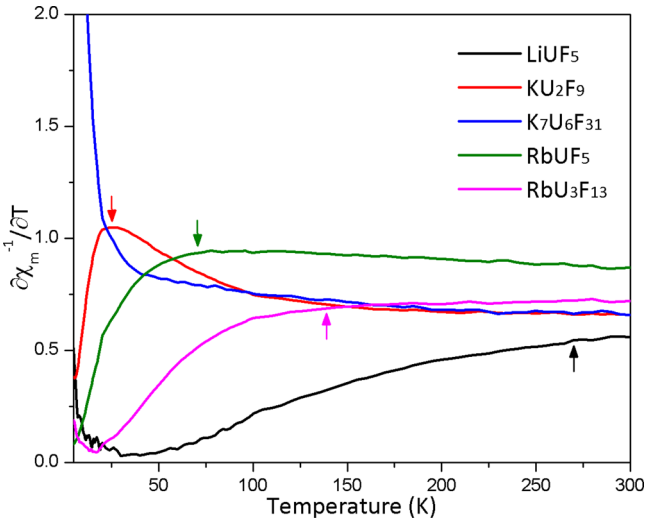

Figure 16. Derivative of the molar inverse susceptibility data as a function of temperature, where the arrows indicate the transitions from triplet to singlet states of the U^{4+}.

susceptibility vs temperature data is plotted in Figure 16, identifying the temperature of the triplet to singlet state transitions of the U^{4+} cation by arrows. KU_2F_9 exhibits a slight upturn around the transition that is reproducible between samples. Interestingly, $K_7U_6F_{31}$ appears to be an exception among the reported group. The rapid increase in the susceptibility with decreasing temperature behavior can be interpreted as being due to persistent paramagnetic moments. The reason for this unusual magnetic behavior of $K_7U_6F_{31}$ is unclear, especially when compared to the structurally related ammonium analogue, $(NH_4)_7U_6F_{31}$[15], that exhibits the expected nonmagnetic ground state of U^{4+}. In this study, we merely suggest two possibilities. First, the unexpected magnetic property of $K_7U_6F_{31}$ may be resulted from an undetected paramagnetic impurity, masking the typical magnetic characteristic of the U^{4+} at low temperature. We find exactly the same behavior for samples of different batches, thus we tend to believe that this behavior is not associated with an impurity phase and should be originating from an intrinsic property. Second, the effect could be the result of the unique local coordination environment of the U^{4+} (UF_8 polyhedra) in $K_7U_6F_{31}$, that is distinctly different from the UF_9 polyhedra observed for the other fluorides reported in this paper. We suggest that the local coordination environment produces a different crystal field effect, giving rise to a complex electronic ground state in $K_7U_6F_{31}$, causing the magnetic behavior to be distinctively different from the other materials. Such unusual magnetic behavior has in fact been observed previously in other compounds,[61,62] although the magnetic properties are not identical to those of $K_7U_6F_{31}$. In our opinion, further spectroscopic investigations to study the electronic states of the uranium in $K_7U_6F_{31}$ are warranted.

As shown in Figure S4, with decreasing temperature, the $\chi_m T$ values gradually drop off for all fluorides discussed in this paper and approach zero due to the loss of thermally excited states. All of the magnetic features, except perhaps those of $K_7U_6F_{31}$, can be explained by the fact that U^{4+} tends to attain a nonmagnetic state at low temperatures, resulting in the presence of spin gaps between the triplet and singlet states rather than magnetic exchange interactions between the U^{4+} centers. The behavior of $K_7U_6F_{31}$ may reflect a competition between crystal field effects and spin-orbit coupling, as discussed by others for similar uranium fluoride systems.[61,62]

CONCLUSIONS

Six ternary alkali U(IV) fluorides were successfully synthesized via an in situ reduction step. The U(VI) in the starting reagent was fully reduced to the U(IV) under a dilute hydrofluoric acid environment, and the single crystals were grown, aided by a copper salt. A single crystal X-ray diffraction study revealed that the reported uranium fluorides exhibit complex crystal structures, and the U(IV) cations are found in large coordination environments. The temperature dependent magnetic susceptibility measurements indicate that U(IV) attains a singlet ground state at low temperature. For all cases, no evidence for long-range magnetic ordering was observed down to 2 K.

ASSOCIATED CONTENT

Supporting Information

X-ray data in CIF format, powder XRD patterns, and magnetic property data. These materials are free of charge via the Internet at http://pubs.acs.org.

AUTHOR INFORMATION

Corresponding Author

*E-mail: zurloye@mailbox.sc.edu.

Notes

The authors declare no competing financial interest.

ACKNOWLEDGMENTS

Research supported by the U.S. Department of Energy, Office of Basic Energy Sciences, Division of Materials Sciences and Engineering under Award DE-SC0008664. Magnetic measurements were performed at the University of Houston and support from the National Science Foundation under Award DMR-1149899 is gratefully acknowledged.

REFERENCES

(1) Ladeira, A. C. Q.; Goncalves, J. S.; Morais, C. A. *Environ. Technol.* **2011**, *32*, 127−131.
(2) Andriychuk, V. *J. Energy Power Eng.* **2011**, *5*, 1126−1133.
(3) Vanderhaegen, M.; Janssens-Maenhout, G.; Peerani, P.; Poucet, A. *Nucl. Eng. Des.* **2010**, *240*, 2988−2993.
(4) Kim, K.-T. *J. Nucl. Mater.* **2010**, *404*, 128−137.
(5) Morel, B.; Duperret, B. *J. Fluorine Chem.* **2009**, *130*, 7−10.
(6) McNamara, B.; Scheele, R.; Kozelisky, A.; Edwards, M. *J. Nucl. Mater.* **2009**, *394*, 166−173.
(7) Ordejon, B.; Seijo, L.; Barandiaran, Z. *J. Chem. Phys.* **2007**, *126*, 194712/194711−194712/194718.

(8) Ordejon, B.; Karbowiak, M.; Seijo, L.; Barandiaran, Z. *J. Chem. Phys.* **2006**, *125*, 074511/074511−074511/074519.
(9) Ordejon, B.; Seijo, L.; Barandiaran, Z. *J. Chem. Phys.* **2005**, *123*, 204502/204501−204502/204509.
(10) Kirishima, A.; Kimura, T.; Nagaishi, R.; Tochiyama, O. *Radiochim. Acta* **2004**, *92*, 705−710.
(11) Kirm, M.; Krupa, J. C.; Makhov, V. N.; Negodin, E.; Zimmerer, G.; Gesland, J. Y. *J. Lumin.* **2003**, *104*, 85−92.
(12) Olchowka, J.; Volkringer, C.; Henry, N.; Loiseau, T. *J. Fluorine Chem.* **2013**, *159*, 1−7.
(13) Schmidt, R.; Müller, B. G. *Z. Anorg. Allg. Chem.* **2004**, *630*, 2393−2397.
(14) Cahill, C. L.; Burns, P. C. *Inorg. Chem.* **2001**, *40*, 1347−1351.
(15) Almond, P. M.; Deakin, L.; Mar, A.; Albrecht-Schmitt, T. E. *J. Solid State Chem.* **2001**, *158*, 87−93.
(16) Hermens, R. A.; Driver, P. L.; Pedro, C. V.; Zhang, X. R.; Schlegel, S. C.; Durning, J. M. *J. Fluorine Chem.* **1996**, *77*, 13−14.
(17) Avignant, D.; Mansouri, I.; Sabatier, R.; Cousseins, J. C.; Chevalier, R. *Acta Crystallogr., Sect. B* **1980**, *B36*, 664−666.
(18) Malm, J. G. *J. Inorg. Nucl. Chem.* **1979**, *41*, 1573−1575.
(19) Cousson, A.; Tabuteau, A.; Pages, M.; Gasperin, M. *Acta Crystallogr., Sect. B* **1979**, *B35*, 1198−1200.
(20) Penneman, R. A.; Ryan, R. R.; Rosenzweig, A. *Acta Crystallogr., Sect. B* **1974**, *B30*, 1966−1970.
(21) Penneman, R. A.; Ryan, R. R.; Rosenzweig, A. *Struct. Bonding (Berlin)* **1973**, *13*, 1−52.
(22) Rosenzweig, A.; Ryan, R. R.; Cromer, D. T. *Acta Crystallogr., Sect. B* **1973**, *29*, 460−462.
(23) Kruse, F. H. *J. Inorg. Nucl. Chem.* **1971**, *33*, 1625−1627.
(24) Brunton, G. D. *Acta Crystallogr., Sect. B* **1971**, *27*, 245−247.
(25) Rosenzweig, A.; Cromer, D. T. *Acta Crystallogr., Sect. B* **1970**, *26*, 38−44.
(26) Brunton, G. D. *Acta Crystallogr., Sect. B* **1969**, *25*, 1919−1921.
(27) Brunton, G. D. *Acta Crystallogr., Sect. B* **1969**, *B25*, 2163−2164.
(28) Brunton, G. D. *J. Inorg. Nucl. Chem.* **1967**, *29*, 1631−1636.
(29) Keenan, T. K. *Inorg. Nucl. Chem. Lett.* **1966**, *2*, 153−156.
(30) Zachariasen, W. H. *Acta Crystallogr.* **1954**, *7*, 792−794.
(31) Zachariasen, W. H. *Acta Crystallogr.* **1948**, *1*, 265−268.
(32) Vlaisavljevich, B.; Diaconescu, P. L.; Lukens, W. L., Jr.; Gagliardi, L.; Cummins, C. C. *Organometallics* **2013**, *32*, 1341−1352.
(33) Schnaars, D. D.; Wu, G.; Hayton, T. W. *J. Am. Chem. Soc.* **2009**, *131*, 17532−17533.
(34) Fortier, S.; Melot, B. C.; Wu, G.; Hayton, T. W. *J. Am. Chem. Soc.* **2009**, *131*, 15512−15521.
(35) Yeon, J.; Smith, M. D.; Sefat, A. S.; Tran, T. T.; Halasyamani, P. S.; zur Loye, H.-C. *Inorg. Chem.* **2013**, *52*, 8303−8305.
(36) Yeon, J.; Smith, M. D.; Tapp, J.; Möller, A.; zur Loye, H.-C. *J. Am. Chem. Soc.* **2014**, *136*, 3955−3963.
(37) *SMART*, version 5.630; *SAINT+*, version 6.45; *SADABS*, version 2.10; Bruker Analytical X-ray Systems, Inc.: Madison, WI, 2003.
(38) Dolomanov, O. V.; Bourhis, L. J.; Gildea, R. J.; K, H. A.; Puschmann, H. *J. Appl. Crystallogr.* **2009**, *42*, 339−341.
(39) Sheldrick, G. M. *Acta Crystallogr.* **2008**, *A64*, 112−122.
(40) Kubelka, P.; Munk, F. Z. *Technol. Phys.* **1931**, *12*, 593−601.
(41) Brese, N. E.; O'Keeffe, M. *Acta Crystallogr.* **1991**, *B47*, 192−197.
(42) Brown, I. D.; Altermatt, D. *Acta Crystallogr.* **1985**, *B41*, 244−247.
(43) Burns, J. H.; Ellison, R. D.; Levy, H. A. *Acta Crystallogr., Sect. B* **1968**, *24*, 230−237.
(44) Underwood, C. C.; Mann, M.; McMillen, C. D.; Kolis, J. W. *Inorg. Chem.* **2011**, *50*, 11825−11831.
(45) Yeon, J.; Smith, M. D.; Sefat, A. S.; zur Loye, H.-C. *Inorg. Chem.* **2013**, *52*, 2199−2207.
(46) Binnemans, K.; Couwenberg, I.; De, L. H.; Gorller-Walrand, C.; Adam, J. L. *J. Alloys Compd.* **1999**, *285*, 105−111.
(47) Carnall, W. T.; Liu, G. K.; Williams, C. W.; Reid, M. F. *J. Chem. Phys.* **1991**, *95*, 7194−7203.
(48) Krupa, J. C. *Inorg. Chim. Acta* **1987**, *139*, 223−241.
(49) Rakshit, S. K.; Jat, R. A.; Naik, Y. P.; Parida, S. C.; Singh, Z.; Sen, B. K. *Thermochim. Acta* **2009**, *490*, 60−63.
(50) Hauck, J. *J. Inorg. Nucl. Chem.* **1974**, *36*, 2291−2298.
(51) Saine, M. C. *J. Less-Common Met.* **1989**, *154*, 361−365.
(52) Yagoubi, S.; Obbade, S.; Dion, C.; Abraham, F. *J. Solid State Chem.* **2005**, *178*, 3218−3232.
(53) Sali, S. K.; Kulkarni, N. K.; Sampath, S.; Jayadevan, N. C. *J. Nucl. Mater.* **1994**, *217*, 294−299.
(54) Saad, S.; Obbade, S.; Renard, C.; Abraham, F. *J. Alloys Compd.* **2009**, *474*, 68−72.
(55) Moertl, K. P.; Sutter, J.-P.; Golhen, S.; Ouahab, L.; Kahn, O. *Inorg. Chem.* **2000**, *39*, 1626−1627.
(56) Boudreaux, E. A.; Mulay, L. N. *Theory and Applications of Molecular Paramagnetism*; Wiley: New York, 1976.
(57) Siladke, N. A.; Meihaus, K. R.; Ziller, J. W.; Fang, M.; Furche, F.; Long, J. R.; Evans, W. J. *J. Am. Chem. Soc.* **2011**, *134*, 1243−1249.
(58) Nocton, G.; Pecaut, J.; Mazzanati, M. *Angew. Chem., Int. Ed.* **2008**, *47*, 3040−3042.
(59) Schelter, E. J.; Morris, D. E.; Scott, B. L.; Thompson, J. D.; Kiplinger, J. L. *Inorg. Chem.* **2007**, *46*, 5528−5536.
(60) Evans, W. J.; Miller, K. A.; Ziller, J. W.; Greaves, J. *Inorg. Chem.* **2007**, *46*, 8008−8018.
(61) Almond, P. M.; Deakin, L.; Porter, M. J.; Mar, A.; Albrecht-Schmitt, T. E. *Chem. Mater.* **2000**, *12*, 3208−3213.
(62) Leask, M. J. M.; Osborne, D. W.; Wolf, W. P. *J. Chem. Phys.* **1961**, *34*, 2090−2099.